RESEARCH ARTICLE

Size Matters: What Are the Characteristic Source Areas for Urban Planning Strategies?

Zhi-Hua Wang[1]*, **Chao Fan**[2], **Soe W. Myint**[2], **Chenghao Wang**[1]

1 School of Sustainable Engineering and the Built Environment, Arizona State University, Tempe, AZ, 85287, United States of America, **2** School of Geographical Sciences and Urban Planning, Arizona State University, Tempe, AZ, 85287, United States of America

* zhwang@asu.edu

Abstract

Urban environmental measurements and observational statistics should reflect the properties generated over an adjacent area of adequate length where homogeneity is usually assumed. The determination of this characteristic source area that gives sufficient representation of the horizontal coverage of a sensing instrument or the fetch of transported quantities is of critical importance to guide the design and implementation of urban landscape planning strategies. In this study, we aim to unify two different methods for estimating source areas, viz. the statistical correlation method commonly used by geographers for landscape fragmentation and the mechanistic footprint model by meteorologists for atmospheric measurements. Good agreement was found in the intercomparison of the estimate of source areas by the two methods, based on 2-m air temperature measurement collected using a network of weather stations. The results can be extended to shed new lights on urban planning strategies, such as the use of urban vegetation for heat mitigation. In general, a sizable patch of landscape is required in order to play an effective role in regulating the local environment, proportional to the height at which stakeholders' interest is mainly concerned.

1. Introduction

Densely built environments are excessively warmer than their rural surroundings, a prominent phenomenon known as the "urban heat island" (UHI) effect [1, 2]. The energetic basis of UHI can be attributed to multiple factors, including modified land surface hydrothermal properties, radiative trapping by buildings, modified aerodynamic roughness, reduced evapotranspiration, and anthropogenic heat release [3–7]. Among these contributors, the use of engineered materials, such as concrete, asphalt, brick, etc. for buildings and pavements, is critical in dictating the UHI effect, given the relatively high thermal storage capacity of these materials. The increase of impervious land cover fractions, together with the rapid urbanization observed in the last few decades [8], has altered the flow patterns of thermal energy in the integrated soil-land-atmosphere continuum [1, 9]. For example, the minimum temperature of Phoenix metropolitan, AZ has experienced an increase of 5.5°C from the late 1940s, and a continuously decreased cooling rate during nighttime due to urban expansion [10, 11].

Among the many adverse environmental impacts of UHI are the significant increase of energy use for cooling of residential and commercial buildings [12–14], and impact on human health with increased heat-related morbidity and mortality [15], especially when exacerbated by heat waves [16]. To alleviate the warming effect induced by impervious engineered pavements, urban vegetation has been widely adopted, common practices including urban lawns, green roofs (also known as "ecoroofs"), shade trees, and urban agriculture [17–19]. Urban vegetation, supplied with adequate soil water availability, is capable of reducing environmental temperature through the cooling effect of evapotranspiration. In addition, vegetated landscapes in built environments also help to improve storm water management and air quality, and to conserve native ecosystems [20–22].

The high spatial heterogeneity associated with the presence of a mixture of a wide variety of landscape types in patches, e.g. pavement, vegetation, open space, etc., is closely related to environmental and ecological patterns of urban areas [3, 23, 24]. Of particular importance to this study, the quantification of urban landscape patterns and its scale dependence is of critical importance in determining source areas of the urban warming effect. Mitigating UHI through vegetation naturally leads to the following question: What is the adequate size of vegetation for reducing air temperatures, for improving human thermal comfort, and/or increasing building energy efficiency? We utilize the multiple endmember spectral mixture analysis (MESMA) to generate fractions of vegetation and impervious surfaces for a sequence of source areas and identified the optimal size for achieving the maximal cooling/warming effect.

Correlation analysis is conducted between land cover fractions derived from remotely sensed images and urban warming measures, i.e. the 2-m air temperature, from ground-based measurements from local meteorological stations. Spatial variability of these statistical correlation coefficients was conventionally used to quantify the effect of different urban land cover features (impervious or vegetated) on air temperature variations [25, 26]. By statistically correlating land use land cover (LULC) types with air temperatures, these indices implicitly encode the relative contribution of different land cover types to urban warming, which coincides with the idea of source areas or "footprint" of urban warming. Interestingly, the concept of source areas has been developed independently in the area of micrometeorology, originated from the description of characteristic scale for vertical mixing of scalars in atmospheric boundary layer (ABL) [27]. The source weight function or footprint function is used to mathematically describe the spatial distribution of surface sources (in this case, urban landscapes and their associated thermal storage) and a measured signal at a height in the surface layer (e.g. 2-m air temperature) [28].

Our objective in this paper is to provide a first attempt to unify the concepts and methodology of correlation analysis and footprint model to quantify the source areas of urban warming. Though developed independently in different scientific branches, and of different mathematical nature (one statistical and the other deterministic and mechanistic), the two methods are speculated to point to the same end in characterizing the impact of different landscapes on elevated urban environmental temperatures. We will use meteorological measurements of air temperatures from the Arizona's Meteorological (AZMET) network to validate the numerical predictions. This proof of concept will help us to identify characteristic horizontal lengths (fetches) contributing to urban warming as a function of meteorological conditions and atmospheric stability, and to address fundamental questions such as: are there threshold source areas required for implementation of UHI mitigation strategies (urban lawns, green roofs, cool roofs, etc.)? and how does this source area vary as a function of different practical applications in urban planning (improving human thermal comfort, enhancing building energy efficiency, modifying local atmospheric circulation pattern for pollutant dispersion, etc.)? The extension of the combined methodology is expected to broaden our fundamental understanding of the

energetic basis and governing mechanisms of urban sustainability in support of practitioners' urban planning strategies.

2. Methodology

2.1. Data and study area

Remote sensing provides a valuable tool to quantify, monitor, and predict land cover changes at an unprecedentedly large spatial scale. A Landsat ETM+ image of 30 m spatial resolution was used to generate detailed land cover fraction maps. The image was acquired over the entire Phoenix metropolitan area on April 19, 2000. We selected the study area as our test site because of the wide variety of LULC classes in this region (e.g., residential, commercial, agriculture, lakes, and exposed soil). Six channels, ranging from blue to the short-wave infrared band, were used as the inputs to the MESMA algorithm. We used a pan-sharpened QuickBird data at 60 cm resolution to validate the accuracy of the MESMA output fractions.

The meteorological indicator of urban warming in our study area is the 2-m air temperature in the urban surface layer. The climatic data used in this study was collected from three networks: Arizona Meteorological Network (AZMET), Maricopa County Flood Control District (MCFCD), and Phoenix Realtime Instrumentation for Surface Meteorological Studies (PRISMS) (Fig 1). Collectively, climate data recorded at 21 weather stations were used in our analysis. The dataset encompasses the maximum, minimum, and mean daily air temperature recorded at the 21 weather stations on April 19, 2000, the same date when the satellite image was acquired.

2.2. Spatial distribution of vegetation and impervious surfaces

Linear spectral mixture analysis (SMA), which provides sub-pixel land cover (endmember) fractions, is the most commonly used technique of all subpixel approaches. A standard SMA approach employs an invariable set of endmembers to model all pixels. This assumption could potentially lead to significant errors since the number and type of land cover components are highly variable. The endmembers used in SMA are the same for each pixel, regardless of whether the ground cover types represented by the endmembers are present in the pixel. Unusual land cover types, which may not merit their own land cover endmember, may also be poorly modeled by SMA. In addition, because SMA allows only one endmember per material it does not account for the same material with different spectral responses [29]. Roberts et al. [30] introduced multiple endmember spectral mixture analysis (MESMA), an extension of SMA approach that allows the number and type of endmembers to vary for each pixel within an image. MESMA allows more than one endmember in the scene per ground component, and has proven to be effective in identifying vegetation species and land cover type in Southern California chaparral [31]. Hence, we employed MESMA to quantify impervious, soil, vegetation and shade in the Phoenix metropolitan area; the effectiveness of the method was demonstrated in previous studies [24]. The Pearson correlation between the fraction outputs from MESMA and reference data from Quickbird 60 cm resolution data for soil, impervious, and vegetation were 0.8030, 0.8632, and 0.8496 respectively [32].

2.3. Correlation analysis

For each weather station, we created a buffer around the station. The buffer (Euclidean) distance ranges from 30 m to 990 m with an increment of 60 m, resulting in a total of 17 geographic extents. For simplicity, two landcover types, viz. impervious and vegetation were used to characterize the land cover around each station, following the treatment in the previous
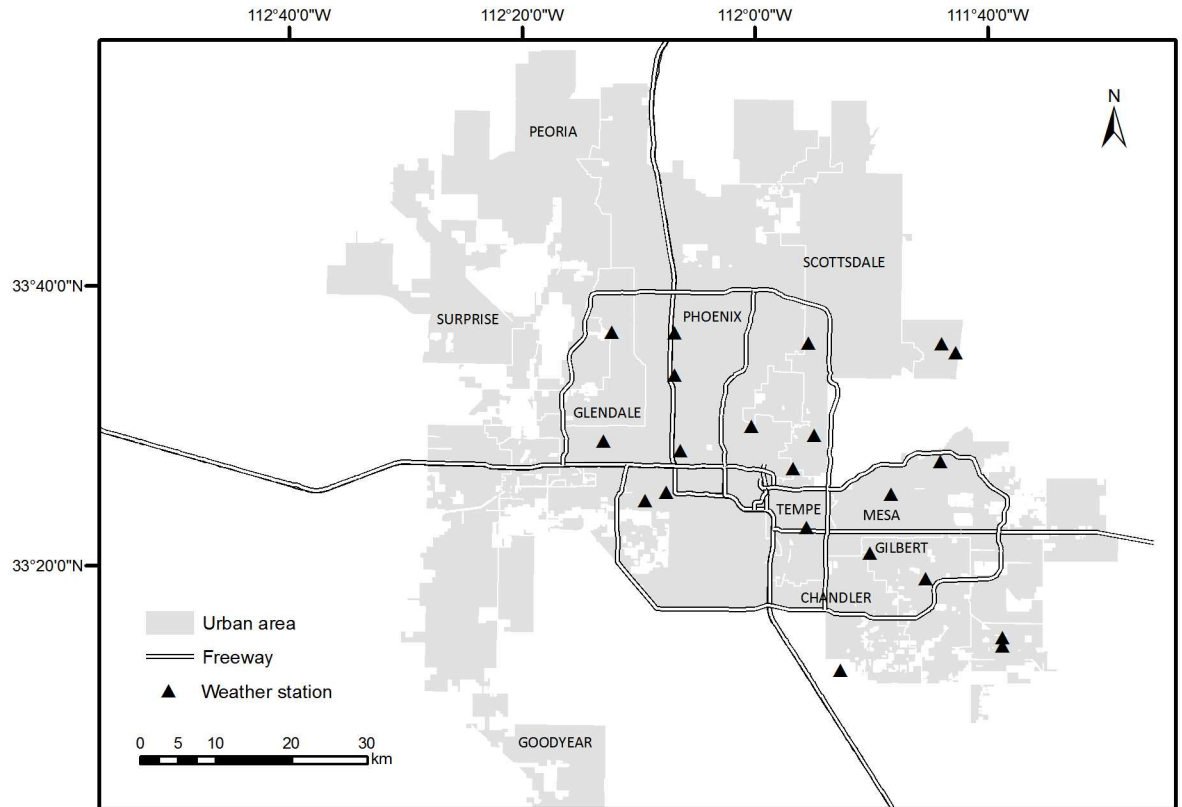
Fig 1. Location of the weather stations in the Phoenix metropolitan area.

study [25]. We then calculated the average land cover fraction within each buffer based on the distribution maps obtained from the MESMA. This composes the observations on one of our covariates x, i.e. the characteristic length of each geographic extent with 60 m increment. The other correlation variable, y, was the maximum/minimum/mean daily air temperature collected from the weather stations.

We used the Pearson product-moment correlation coefficient as our measure of the linear association between the x and y variables. It ranges from -1 to +1, with -1/+1 indicating the perfect negative/positive correlation. Statistically, Pearson's correlation coefficient is defined as

$$\rho(x, y) = \frac{\text{cov}(x, y)}{\sigma_x \sigma_y},$$ (1)

where $\text{cov}(x, y)$ is the covariance between x and y, and σ is the standard deviation. The covariance between x and y is given by

$$\text{cov}(x, y) = E\{[x - E(x)][y - E(y)]\}.$$ (2)

where E is the expected value of a given sample (statistical mean). The Pearson's correlation coefcient was used as an indicator of the linear dependence between the air temperature measured at the weather station and the land cover fraction assessed at a series of spatial extents centered at the station.

PLOS ONE

Size Matters: What Are the Characteristic Source Areas for Urban Planning Strategies?

2.4. Footprint model

There are numerous models, be it analytical, stochastic or mechanistic, in estimating the footprint of scalars and scalar fluxes in the ABL (see. e.g. [28] for a comprehensive review). Here we adopt a widely-used and extensively tested analytical model developed by Kormann and Meixner [33]. In this model, the distributed concentration footprint of a scalar (e.g. temperature, humidity, concentration of pollutants, etc.) mixing along x direction (orientated along the wind direction) is given by

$$c(x, z) = \frac{1}{\Gamma(\mu)} \frac{r}{Uz^{1+m}} \frac{\xi^\mu}{x^\mu} e^{-\xi/x}, \tag{3}$$

where Γ is the gamma function; $r = 2 + m - n$ is the shape factor with m and n the exponents of the power laws describing the vertical proles of wind speed u and eddy diffusivity K, via $u(z) = Uz^m$, and $K(z) = kz^n$ with k a constant coefcient in the power law prole; $\mu = (1 + m) / r$; U is the constant in power-law prole of the wind velocity; z is the height; and ξ is the characteristic length scale dened by

$$\xi(z) = \frac{Uz^r}{r^2 \kappa}, \tag{4}$$

with κ the von Karman constant (0.4). The key of the analytical model is to determine the exponents m and n, by relating the power law to Monin-Obukhov similarity theory (MOST) for the horizontal wind, as

$$m = \frac{z}{u} \frac{du}{dz} = \frac{u_*}{u\kappa} \varphi_m, \tag{5}$$

and

$$n = \frac{z}{K} \frac{dK}{dz} = \begin{cases} \dfrac{1}{1 + 5z/L} & \text{for } L > 0 \\ \dfrac{1 - 24z/L}{1 - 16z/L} & \text{for } L < 0 \end{cases}, \tag{6}$$
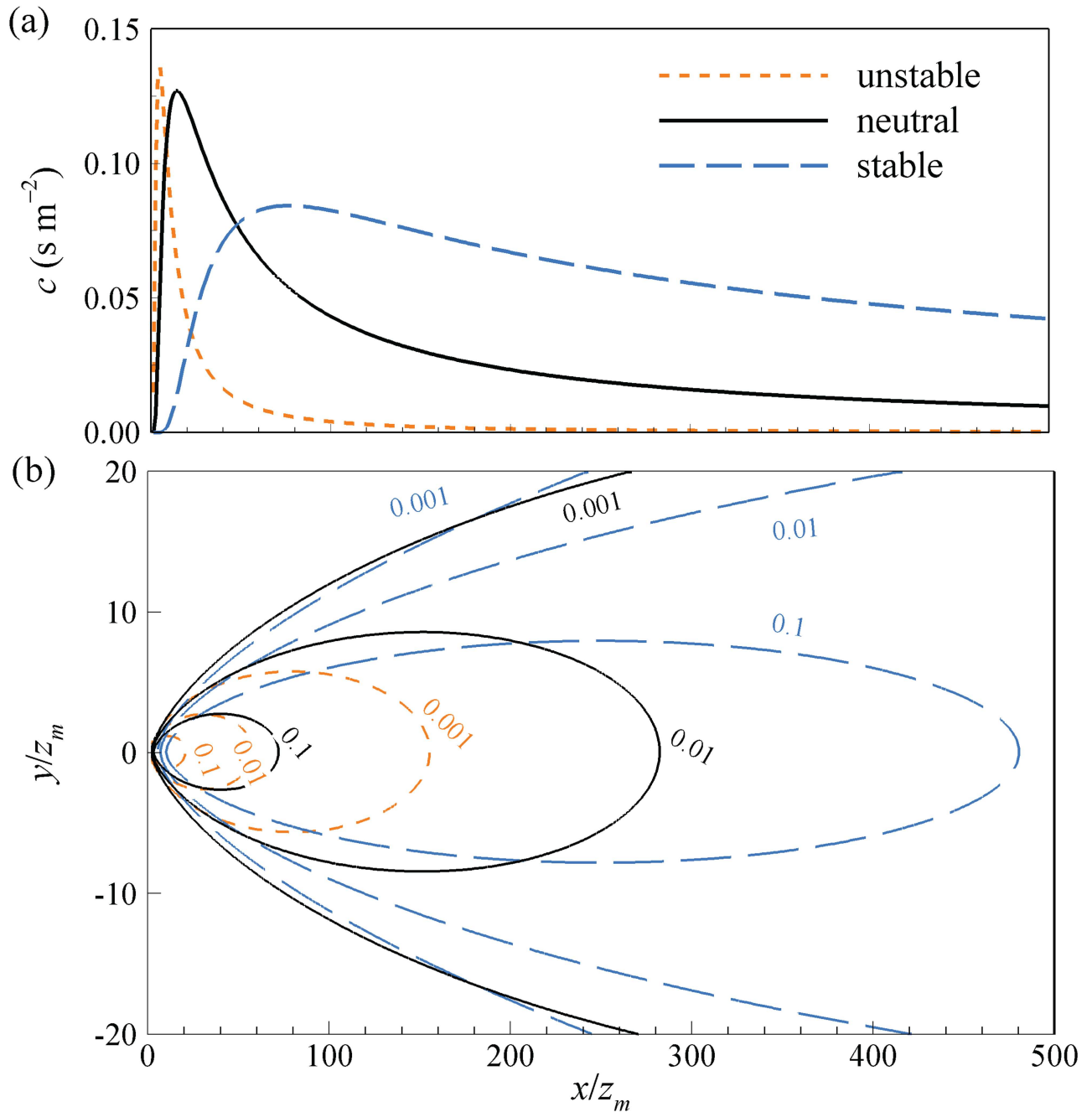
where u_* is the friction velocity, L is the Obukhov length for measuring dynamic stability of the surface layer (viz. the dimensional height $z/L > 0$ for stable atmosphere, $z/L < 0$ unstable, and $z/L = 0$ neutral), and φ_m is the stability function following the Businger-Dyer relationship [34]:

$$\varphi_m = \begin{cases} 1 + 5z/L & \text{for } L > 0 \\ (1 - 16z/L)^{-1/4} & \text{for } L < 0 \end{cases}. \tag{7}$$

In addition, the crosswind distributed concentration footprint is given by,

$$\gamma(x, y, z) = D_y c(x, z) = \frac{1}{\sqrt{2\pi}\sigma} e^{-\frac{y^2}{2\sigma^2}} \frac{1}{\Gamma(\mu)} \frac{r}{Uz^{1+m}} \frac{\xi^\mu}{x^\mu} e^{-\xi/x}, \tag{8}$$

where D_y is the crosswind distribution function, and σ the dispersion. Fig 2 depicts sample plots of the footprint functions as integrated over the crosswind direction as well as the lateral distributions. It is clear that as the atmospheric instability increases (i.e. more turbulent weather conditions), the concentration of a scalar distributes over a more widely spread area, leading to a larger footprint of the scalar.

PLOS | ONE

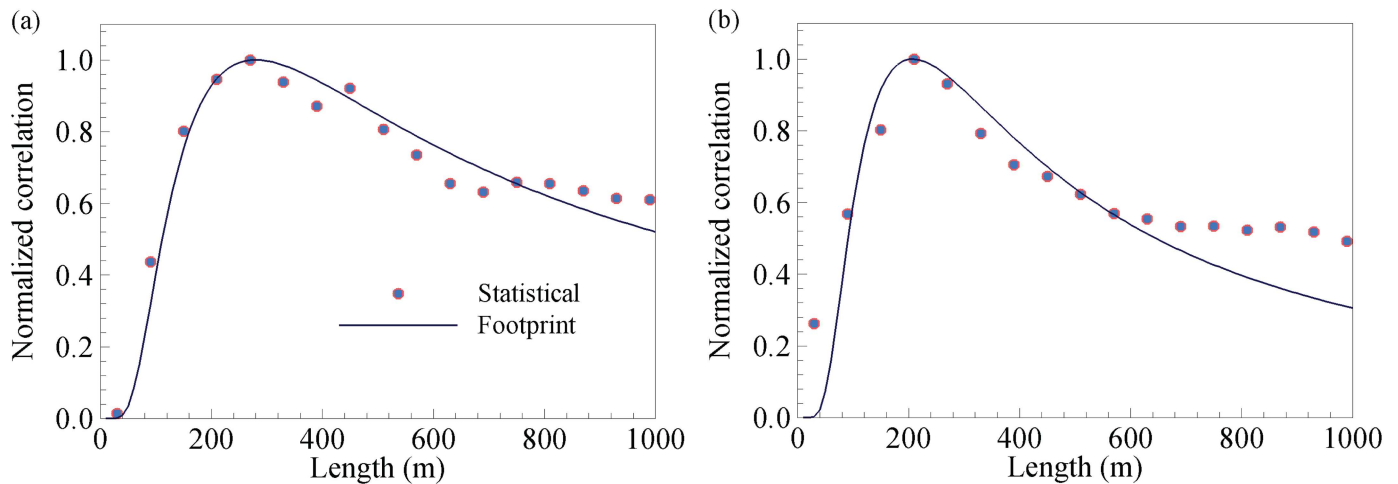Size Matters: What Are the Characteristic Source Areas for Urban Planning Strategies?

Fig 2. Sample plots of (a) the crosswind integrated footprint function, and (b) isopleths of the footprint with lateral distribution, with the numbers on the isopleths indicating the contour of constant values of crosswind integrated footprint.

3. Results and Discussion

[Fig 3](#) shows the sample result of comparison between the normalized statistical correlations (of the maximum air temperatures recorded by 21 AZMET stations shown in [Fig 1](#) on a typical clear day April 19, 2000 in Phoenix and 17 LULC pixels), and the normalized temperature footprint using the analytical model in Section 2.4. The turbulent and aerodynamic parameters used in estimating the footprint, viz. friction velocity u_*, Obukhov length L, and roughness

PLOS ONE

Size Matters: What Are the Characteristic Source Areas for Urban Planning Strategies?

Fig 3. Intercomparison of the normalized correlation between the air temperature and LULC types for (a) vegetation and (b) impervious surfaces at the study site and the normalized footprint, on April 19, 2000. (The average turbulent field data for estimating the footprint are: friction velocity $u_* = 0.2$ m s^{-1}, dynamic stability $z/L = -0.2$ unstable, and roughness length $z_0 = 0.05$ m).

doi:10.1371/journal.pone.0165726.g003

length z_0, were determined based on measurements from an eddy-covariance tower and a network of weather stations, reported in previous studies [35, 36]. We have conducted similar comparisons between results of the two models under a variety of environmental conditions, including wind directions, weather conditions, atmospheric stability, and other indicators (e.g. minimum or mean temperatures). Most of the comparisons show very similar agreement (not shown here, a complete set of plots of statistical correlation can be found in [25]). This is a pioneering effort linking urban temperature with the contributing source areas at different sizes predicted by two vastly different models: one based on empirical relations (statistical correlation of measurements) and the other on mechanistic turbulence resolution. Both correlation and footprint are normalized by their maximum values (i.e. $y_{normalized} = y/y_{max}$), so to yield the maximum of unity for intercomparison. The agreement between the two methods is reasonably good. Both methods estimate that for the recorded daily maximum air temperature, the maximum contribution is from a source area of around 200 m × 200 m for vegetated and impervious surfaces. Note that the statistical correlations are negative for vegetated surfaces (we plot the absolute values in Fig 3a) and positively for impervious surfaces. This is physical in that urban vegetation tends to mitigate the maximum air temperature by evapotranspirative cooling, whereas the impervious surfaces (mainly engineering pavements) contributes positively to urban warming.

The longer tails observed in the statistical correlations in Fig 3(b), is mainly due to the inhomogeneity of the built landscape. The presence of adjacent built structures (e.g. rooftops) within ~1 km range of the weather stations, which are of similar material properties to impervious surfaces in canyons, likely contribute more to the scalar transport than flat patches due to their elevated heights (so they contribute as stronger "surface" sources). The actual correlation of 2-m air temperature measurement at ground level with its source areas, therefore, exhibits a "folding" or reflection of the scalar contribution due to the neighboring structures, a phenomenon analogous to the aliasing error due to high frequency filtering [37]. On the other hand, note that the analytical footprint model is derived for homogenous surface terrains assuming stationary turbulence, where surface obstacles are treated as homogeneous roughness elements. Thus the contribution from adjacent buildings predicted by the footprint model is smoother and has a faster decay at the tail. This discrepancy between the two methods

at the tail within 1 km is likely to be weakened when we move further away from the measurement points, where temperature contribution further decreases, and the impact of surface inhomogeneity will fade as well.

As shown in Fig 3, the maximum footprint f_{max} (or maximum statistical correlation ρ_{max}) occurs at certain source area (upwind in the footprint model) with horizontal dimension x_{max}. Both are strong functions of the measurement height of the sensing instrument above the land surface. Whereas empirically there is no *a priori* knowledge existed in order to predicted these relations, the analytical footprint model offers a good clue. According to the formulation presented in Section 2.4, it can be readily derived that the maximum laterally-integrated footprint is given by [33] as

$$f_{max} = \frac{(1+\mu)^{1+\mu}}{\Gamma(\mu)\xi} e^{-1-\mu},$$ (9)

which is found at the upwind distance of

$$x_{max} = \frac{\xi}{1+\mu},$$ (10)

from the location of the station. The height-dependent footprint distribution is sketched in Fig 4. As the measurement height increases, the characteristic horizontal length increases (usually nonlinearly) as well. Given the agreement between the results of the footprint model, this relation can be readily extended (at least qualitatively) to predict the statistical correlation between measured meteorological variables (not limited to ambient temperatures) and the contributing LULC types. Thus the result of footprint model offers valuable estimates of the adequate sizes of grid-cells (e.g. the coarsest spatial resolution should at least resolve the characteristic length x_{max} which represents the maximum correlation) for landscape fragmentation for various geophysical studies.

This source-area-to-measurement-height relation, when closely scrutinized, can have profound implications to urban planning in determining the threshold size of, e.g. vegetation patches for mitigating urban warming. For the particular sites in this study, subjected to local climatological, geophysical, and environmental conditions, the recorded daily maximum temperature using the AZMET stations is most strongly regulated by upwind patches of ~ 100 m in size, negatively by vegetation and positively by impervious surfaces. It can be extended that if urban planners' primary concerns shift case-by-case, e.g. from enhancing pedestrian's thermal comfort in street canyons to alleviating environmental thermal stress in urban boundary layer. With the due increase of "height of interest" (here in the sense of the average height at which stakeholders' interest is mainly concerned), the optimal size of source areas, by estimation, will increase accordingly by a few folds to, e.g. ~ 500–1000 m. This is rather commonplace as we found in hot summer days, patches of lawns and swimming pools of typical characteristic lengths of 10–20 m in residential areas offer comfortable cooling to pedestrians. It also appeals to our physical intuition that a car park paved of asphalt can lead to elevated thermal stress as well as building cooling cost in its vicinity, at a height proportional to its size.

This concept is further illustrated schematically in Fig 4, where four urban planning strategies for four applications with distinctive scales are plotted. These include (I) the sub-meter scale (~ 0.1 m, vertical scale, same hereinafter) turbulent transport that dominants the rate of mixing and dissipation, e.g. mixing of pollutant in street canyons or nocturnal cooling of building facades, (II) the pedestrian scale (~ 1 m) thermal states, e.g. the estimate of outdoor human comfort indices, (III) the building scale (~10 m) interactions with the environment, e.g. energy saving by tree shading, and (IV) the atmospheric boundary layer (ABL) scale

PLOS | ONE

Size Matters: What Are the Characteristic Source Areas for Urban Planning Strategies?
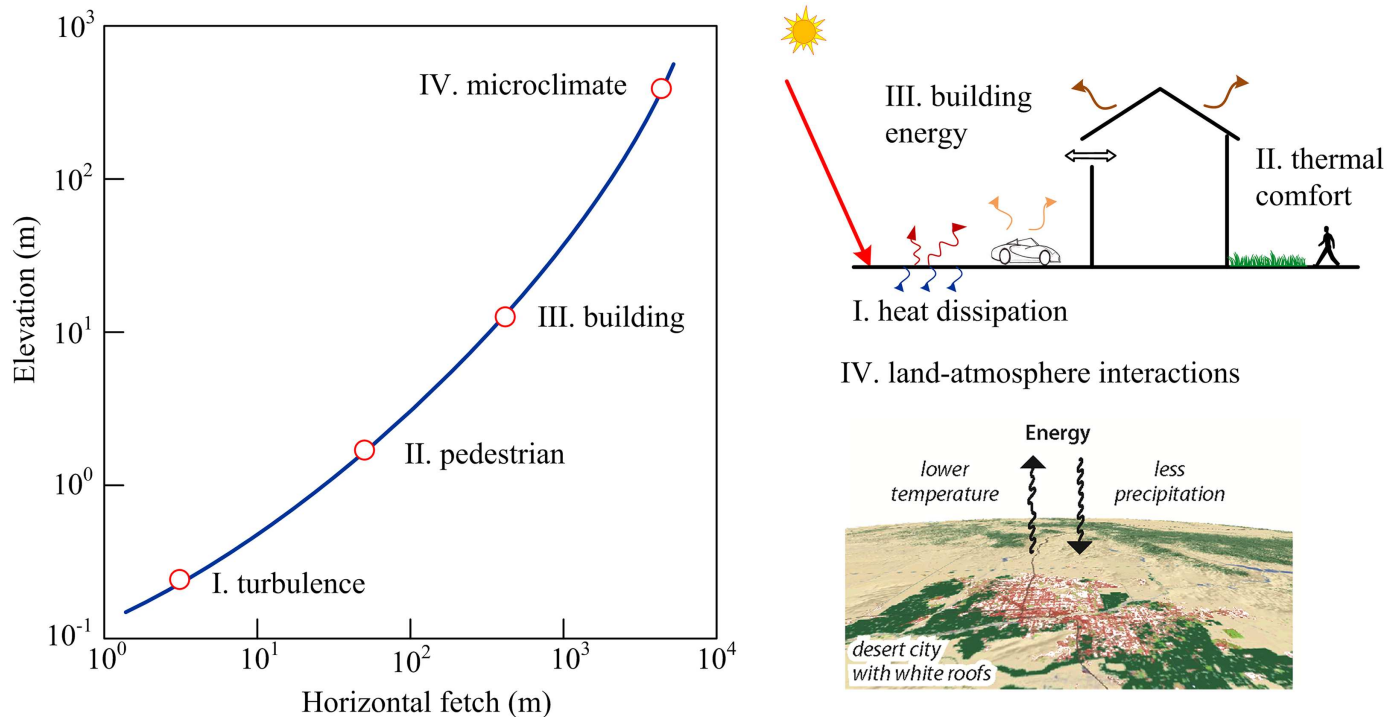
Fig 4. Illustration of the relationship between the measurement height and the characteristic horizontal distance (source area size), with examples at different scale of real applications, including (I) turbulent scale heat dissipation, (II) outdoor thermal comfort, (III) building energy efficiency, and (IV) urban microclimate modeling.

(~100–1000 m) microclimate, e.g. urban-land-atmosphere interactions or pollutant dispersion over the city. Depending on the actual application that concerns homeowners, practitioners, or resource managers, the corresponding source areas (e.g. the patch size of urban lawns or sizes of landscape fragmentation) need to be carefully selected in order to yield the desirable effect of landscape planning.

4. Concluding Remarks

This study presents a pioneering study in estimating the dependence of urban temperature measurement on characteristic horizontal length, viz. the source area, by unifying the statistical correlation method commonly used in geographical science with the analytical footprint model in meteorological and environmental studies. There is a good agreement between numerical predictions of the two methods, based on weather station measurements in a typical clear day in Phoenix Arizona. It is noteworthy that due to the practical limitation in urban meteorological measurements, especially the lack of wide spectrum in measurement height, results of the current study are constrained to the 2-m air temperature as the signal variable of turbulent transport. In addition, the current results are based on a diurnal measurement (24 hours), where the determination of analytical footprint depends heavily upon the site-specific and time-specific meteorological and flow conditions, especially the prevailing wind direction, friction velocity, and atmospheric stability. Nevertheless, if longterm urban climatology of various cities is considered in real applications, the result of the current study can be readily extended or even simplified. For example, for a design of inter-city transportation network and its impact on regional climate, the prevailing wind direction is likely disappear when large geographic variability is covered, and an directional average of footprint estimate over 360° in

the designated region may suffice. Hence, the results of this study can be extended to guide the design of various urban planning strategies, as well as to achieve optimal implementation of urban infrastructure where multiple applications with different scale need to be considered for trade-offs.

Acknowledgments

Author Contributions

Conceptualization: ZHW.

Data curation: ZHW SM.

Formal analysis: ZHW CF SM CW.

Funding acquisition: ZHW SM.

Investigation: ZHW CF SM CW.

Methodology: ZHW CF SM CW.

Project administration: ZHW.

Resources: ZHW SM.

Software: ZHW CF SM CW.

Supervision: ZHW SM.

Validation: ZHW CF SM CW.

Visualization: ZHW CF SM CW.

Writing – original draft: ZHW CF SM CW.

Writing – review & editing: ZHW CF SM CW.

References

1. Oke TR. The energetic basis of the urban heat island. Q J R Meteorol Soc. 1982; 108(455):1–24. doi: 10.1002/qj.49710845502

2. Taha H. Urban climates and heat islands: Albedo, evapotranspiration, and anthropogenic heat. Energy Build. 1997; 25(2):99–103. doi: 10.1016/s0378-7788(96)00999-1

3. Arnfield AJ. Two decades of urban climate research: A review of turbulence, exchanges of energy and water, and the urban heat island. Int J Climatol. 2003; 23(1):1–26. doi: 10.1002/joc.859

4. Narumi D, Kondo A, Shimoda Y. Effects of anthropogenic heat release upon the urban climate in a Japanese megacity. Environ Res. 2009; 109(4):421–31. doi: 10.1016/j.envres.2009.02.013 PMID: 19349044

5. Sailor DJ. A review of methods for estimating anthropogenic heat and moisture emissions in the urban environment. Int J Climatol. 2011; 31(2):189–99. doi: 10.1002/joc.2106

6. Wang ZH. A new perspective of urban-rural differences: The impact of soil water advection. Urban Clim. 2014; 10:19–34.

7. Wang ZH. Monte Carlo simulations of radiative heat exchange in a street canyon with trees. Solar Energy. 2014; 110:704–13. doi: 10.1016/j.solener.2014.10.012

8. United Nations (UN). World urbanization prospects: The 2014 revision. New York: The United Nations' Department of Economic and Social Affairs—Population Division, Division DoEaSAP; 2014 Contract No.: ST/ESA/SER.A/352.

9. Fischer EM, Seneviratne SI, Luthi D, Schar C. Contribution of land-atmosphere coupling to recent European summer heat waves. Geophys Res Lett. 2007; 34(6):L06707. doi: 10.1029/2006gl029068

10. Brazel A, Selover N, Vose R, Heisler G. The tale of two climates—Baltimore and Phoenix urban LTER sites. Clim Res. 2000; 15(2):123–35. doi: 10.3354/cr015123

11. Lee T-W, Lee JY, Wang ZH. Scaling of the urban heat island intensity using time-dependent energy balance. Urban Clim. 2012; 2:16–24. doi: 10.1016/j.uclim.2012.10.005

12. Santamouris M, Papanikolaou N, Livada I, Koronakis I, Georgakis C, Argiriou A, et al. On the impact of urban climate on the energy consumption of buildings. Solar Energy. 2001; 70(3):201–16. doi: 10.1016/S0038-092X(00)00095-5

13. Kolokotroni M, Zhang YP, Watkins R. The London heat island and building cooling design. Solar Energy. 2007; 81(1):102–10. doi: 10.1016/j.solener.2006.06.005

14. Yang J, Wang ZH, Kaloush KE. Environmental impacts of reflective materials: Is high albedo a 'silver bullet' for mitigating urban heat island? Renew Sustain Energy Rev. 2015; 47:830–43.

15. Patz JA, Campbell-Lendrum D, Holloway T, Foley JA. Impact of regional climate change on human health. Nature. 2005; 438(7066):310–7. doi: 10.1038/nature04188 PMID: 16292302

16. Fouillet A, Rey G, Laurent F, Pavillon G, Bellec S, Guihenneuc-Jouyaux C, et al. Excess mortality related to the August 2003 heat wave in France. Int Arch Occup Environ Health. 2006; 80(1):16–24. doi: 10.1007/s00420-006-0089-4 PMID: 16523319

17. Yang J, Wang ZH. Physical parameterization and sensitivity of urban hydrological models: Application to green roof systems. Build Environ. 2014; 75:250–63. doi: 10.1016/j.buildenv.2014.02.006

18. Song J, Wang ZH. Impacts of mesic and xeric urban vegetation on outdoor thermal comfort and microclimate in Phoenix, AZ. Build Environ. 2015; 94(2):558–68. doi: 10.1016/j.buildenv.2015.10.016

19. Wang ZH, Zhao X, Yang J, Song J. Cooling and energy saving potentials of shade trees and urban lawns in a desert city. Appl Energy. 2016; 161(3):437–44. doi: 10.1016/j.apenergy.2015.10.047

20. Oberndorfer E, Lundholm J, Bass B, Coffman RR, Doshi H, Dunnett N, et al. Green roofs as urban ecosystems: Ecological structures, functions, and services. Bioscience. 2007; 57(10):823–33. doi: 10.1641/b571005

21. Dvorak B, Volder A. Green roof vegetation for North American ecoregions: A literature review. Landscape Urban Plan. 2010; 96(4):197–213. doi: 10.1016/j.landurbplan.2010.04.009

22. Yang J, Wang ZH, Georgescu M, Chen F, Tewari M. Assessing the impact of enhanced hydrological processes on urban hydrometeorology with application to two cities in contrasting climates. Journal of Hydrometeorology. 2016; 17:1031–47. doi: 10.1175/JHM-D-15-0112.1

23. Buyantuyev A, Wu JG. Urban heat islands and landscape heterogeneity: linking spatiotemporal variations in surface temperatures to land-cover and socioeconomic patterns. Landsc Ecol. 2010; 25(1):17–33. doi: 10.1007/s10980-009-9402-4

24. Fan C, Myint SW, Zheng BJ. Measuring the spatial arrangement of urban vegetation and its impacts on seasonal surface temperatures. Progr Phys Geograph. 2015; 39(2):199–219. doi: 10.1177/0309133314567583

25. Myint SW, Brazel A, Okin G, Buyantuyev A. Combined effects of impervious surface and vegetation cover on air temperature variations in a rapidly expanding desert city. GISci Remote Sens. 2010; 47(3):301–20.

26. Chen XL, Zhao HM, Li PX, Yin ZY. Remote sensing image-based analysis of the relationship between urban heat island and land use/cover changes. Remote Sens Environ. 2006; 104(2):133–46. doi: 10.1016/j.rse.2005.11.016

27. Pasquill F. Some aspects of boundary layer description. Q J R Meteorol Soc. 1972; 98(417):469–94.

28. Schmid HP. Footprint modeling for vegetation atmosphere exchange studies: a review and perspective. Agric Forest Meteorol. 2002; 113(1–4):159–83. doi: 10.1016/s0168-1923(02)00107-7

29. Myint SW, Lam NSN, Tyler JM. Wavelets for urban spatial feature discrimination: Comparisons with fractal, spatial autocorrelation, and spatial co-occurrence approaches. Photogramm Eng Remote Sens. 2004; 70(7):803–12. doi: 10.14358/PERS.70.7.803

30. Roberts DA, Gardner M, Church R, Ustin S, Scheer G, Green RO. Mapping chaparral in the Santa Monica Mountains using multiple endmember spectral mixture models. Remote Sens Environ. 1998; 65(3):267–79. doi: 10.1016/s0034-4257(98)00037-6

PLOS ONE

Size Matters: What Are the Characteristic Source Areas for Urban Planning Strategies?

31. Dennison PE, Roberts DA, Regelbrugge JC. Characterizing chaparral fuels using combined hyperspectral and synthetic aperture radar. Proceedings of the Ninth JPL Airborne Earth Science Workshop; Pasadena, CA: Jet Propulsion Laboratory; 2000. p. 119–24.

32. Myint SW, Okin GS. Modelling land-cover types using multiple endmember spectral mixture analysis in a desert city. Int J Remote Sens. 2009; 30(9):2237–57. doi: 10.1080/01431160802549328

33. Kormann R, Meixner FX. An analytical footprint model for non-neutral stratification. Bound-Layer Meteor. 2001; 99(2):207–24. doi: 10.1023/a:1018991015119

34. Dyer AJ. A review of flux-profile relationships. Bound-Layer Meteor. 1974; 7:363–72.

35. Wang ZH, Bou-Zeid E, Smith JA. A coupled energy transport and hydrological model for urban canopies evaluated using a wireless sensor network. Q J R Meteorol Soc. 2013; 139(675):1643–57. doi: 10.1002/qj.2032

36. Chow WT, Volo TJ, Vivoni ER, Jenerette GD, Ruddell BL. Seasonal dynamics of a suburban energy balance in Phoenix, Arizona. International Journal of Climatology. 2014; 34(15):3863–80. doi: 10.1002/joc.3947

37. Stull RB. An introduction to boundary layer meteorology. Dordrecht: Kluwer Academic Publishers; 1988. 670 p.